



1  **$^{14}\text{C}$  observations of atmospheric  $\text{CO}_2$  at Anmyeondo GAW**  
2 **station, Korea: Implications for fossil fuel  $\text{CO}_2$  and emission**  
3 **ratios**

4 Haeyoung Lee<sup>1,2</sup>, Edward J. Dlugokencky<sup>3</sup>, Jocelyn C Turnbull<sup>4,5</sup>, Sepyo Lee<sup>1</sup>, Scott J. Lehman<sup>6</sup>,  
5 John B Miller<sup>3</sup>, Gabrielle Petron<sup>3,5</sup>, Jeongsik Lim<sup>7</sup>, Gang-Woong Lee<sup>2</sup>, Sang-Sam Lee<sup>1</sup> and  
6 Young-San Park<sup>1</sup>

7  
8 Correspondence to Haeyoung Lee ([leehy80@korea.kr](mailto:leehy80@korea.kr))

9

10 <sup>1</sup>National Institute of Meteorological Sciences, Jeju, 63568, Republic of Korea

11 <sup>2</sup>Atmospheric Chemistry Laboratory, Hankuk University of Foreign Studies, Gyeonggi-do, 17035, Republic of  
12 Korea

13 <sup>3</sup>NOAA, Earth System Research Laboratory, Global Monitoring Division, Boulder, Colorado, USA

14 <sup>4</sup>National Isotope Center, GNS Science, Lower Hutt, New Zealand

15 <sup>5</sup>CIRES, University of Colorado, Boulder, Colorado, USA

16 <sup>6</sup>INSTAAR, University of Colorado, Boulder, Colorado, USA

17 <sup>7</sup>Korea Research Institute of Standard and Science, Daejeon, 34113, Republic of Korea

18

19 *Abstract. To understand Korea's carbon dioxide ( $\text{CO}_2$ ) emissions and sinks as well as those of*  
20 *the surrounding region, we used 70 flask-air samples collected during May 2014 to August 2016*  
21 *at Anmyeondo (AMY, 36.53° N, 126.32° E; 46 m a.s.l.) World Meteorological Organization*  
22 *(WMO) Global Atmosphere Watch (GAW) station, located on the west coast of South Korea, for*  
23 *analysis of observed  $^{14}\text{C}$  in atmospheric  $\text{CO}_2$  as a tracer of fossil fuel  $\text{CO}_2$  contribution ( $C_{\text{ff}}$ ).*  
24 *Observed  $^{14}\text{C}/\text{C}$  ratios in  $\text{CO}_2$  at AMY varied from -59.5 to 23.1‰ with the measurement*  
25 *uncertainty of  $\pm 1.8\%$ . The derived mean value  $C_{\text{ff}}$  of  $(9.7 \pm 7.8) \mu\text{mol mol}^{-1}$  ( $1\sigma$ ) is greater than*  
26 *that found in earlier observations from Tae-Ahn Peninsula (TAP, 36.73° N, 126.13° E, 20 m*  
27 *a.s.l., 24 km away from AMY) of  $(4.4 \pm 5.7) \mu\text{mol mol}^{-1}$  from 2004 to 2010. The enhancement*  
28 *above background of sulfur hexafluoride ( $\Delta x(\text{SF}_6)$ ) and carbon monoxide ( $\Delta x(\text{CO})$ ) correlate*  
29 *strongly with  $C_{\text{ff}}$  ( $r > 0.7$ ) and appear to be good proxies for fossil fuel  $\text{CO}_2$  at regional and*



30 *continental scales. Samples originating from the Asian continent had greater  $\Delta x(\text{CO}):C_{\text{ff}}(R_{\text{CO}})$*   
31 *values,  $(29 \pm 8)$  to  $(36 \pm 2)$   $\text{nmol } \mu\text{mol}^{-1}$ , than in Korean local air  $((8 \pm 2) \text{ nmol } \mu\text{mol}^{-1})$ . Air masses*  
32 *originating in China showed  $(1.8 \pm 0.2)$  times greater  $R_{\text{CO}}$  than a bottom-up inventory suggesting*  
33 *that China's CO emissions are underestimated in the inventory. However, both  $R_{\text{CO}}$  derived from*  
34 *inventories and observations have decreased relative to previous studies, indicating that*  
35 *combustion efficiency is increasing in both China and South Korea.*

## 36 **1 Introduction**

37 Carbon Dioxide ( $\text{CO}_2$ ) is the principle cause of climate change in the industrial era, and is  
38 increasing in the atmosphere at  $(2.4 \pm 0.5) \mu\text{mol mol}^{-1} \text{ a}^{-1}$  in a recent decade globally  
39 ([www.esrl.noaa.gov/gmd/ccgg/trends/](http://www.esrl.noaa.gov/gmd/ccgg/trends/), last access: 6 December 2019). This increase is in fact  
40 predominantly an anthropogenic disturbance that has been demonstrated through  $^{14}\text{C}$  analysis of  
41 tree rings from the last two centuries (Stuiver and Quay, 1981; Suess, 1955; Tans et al., 1979),  
42 caused by accelerated release of  $\text{CO}_2$  from fossil fuel burning. Atmospheric measurement  
43 program for the ratio  $^{14}\text{C}/\text{C}$  in  $\text{CO}_2$  was initiated in the 1950s and 1960s (Rafter and Fergusson,  
44 1957; Nydal, 1996). Observed  $^{14}\text{C}/\text{C}$  ratios are reported in Delta notation ( $\Delta(^{14}\text{CO}_2)$ ) as  
45 fractionation-corrected permil (or ‰) deviations from the absolute radiocarbon standard  
46 (Stuiver and Polach, 1977). Many studies show that the variation of  $\Delta(^{14}\text{CO}_2)$  is an unbiased and  
47 now widely used tracer for  $\text{CO}_2$  emitted from fossil-fuel combustion (Levin et al., 2003; Turnbull  
48 et al., 2006; Graven et al., 2009; Miller et al., 2012). Therefore measurements of  $\Delta(^{14}\text{CO}_2)$  are  
49 important to test the effectiveness of emission reduction strategies to mitigate the rapid



50 atmospheric CO<sub>2</sub> increase, since they can partition observed CO<sub>2</sub> enhancements,  $\Delta x(\text{CO}_2)$ , into  
51 fossil fuel CO<sub>2</sub> ( $C_{\text{ff}}$ ) and biological CO<sub>2</sub> ( $C_{\text{bio}}$ ) components with high confidence (Turnbull et al.,  
52 2006).

53 When trace gases are co-emitted with  $C_{\text{ff}}$ , correlations of their enhancements with  $C_{\text{ff}}$  improve  
54 understanding of the emission sources of both  $C_{\text{ff}}$  and the co-emitted tracers. For example, CO  
55 and CH<sub>4</sub> emission inventories are typically more uncertain than the fossil fuel CO<sub>2</sub> emission  
56 inventory, since those emissions related to complete combustion are generally well estimated  
57 while emissions related to incomplete combustion and agricultural activities are poorly  
58 constrained (Kurokawa et al., 2013). Temporal changes in the observed emission ratio of a trace  
59 gas to  $C_{\text{ff}}$  can be used to examine emission trends in the trace gas (Tohijima et al., 2014).  
60 Therefore the observed emission ratios of trace gases to  $C_{\text{ff}}$  can be used to evaluate bottom-up  
61 inventories of various trace gases (e.g., Miller et al., 2012). Here, we used two trace gases,  
62 carbon monoxide (CO) and sulfur hexafluoride (SF<sub>6</sub>) for this analysis. CO is produced along  
63 with CO<sub>2</sub> during incomplete combustion of fossil fuels and biomass. CO enhancements above  
64 background ( $\Delta x(\text{CO}_2)$ ) correlate well with  $C_{\text{ff}}$  and have been used as a fossil fuel tracer  
65 (Gamnitzer et al., 2006; Turnbull et al., 2011a; Turnbull et al., 2011b; Tohijima et al., 2014). SF<sub>6</sub>  
66 is an entirely anthropogenic gas and is widely used as an arc quencher in high-voltage electrical  
67 equipment (Geller et al., 1997). At regional to continental scales, persistent small leaks to the  
68 atmosphere of SF<sub>6</sub> are typically co-located with fossil fuel CO<sub>2</sub> sources and allow SF<sub>6</sub> to be used  
69 as an indirect  $C_{\text{ff}}$  tracer, if the leaks are co-located with  $C_{\text{ff}}$  emissions at the location and scale of  
70 interest (Turnbull et al., 2006; Rivier et al., 2006).

71 South Korea is a rapidly developing country with fast economic growth, and it is located next to  
72 China, which is the world's largest emitter of anthropogenic CO<sub>2</sub>, according to the Emissions



73 Database for Global Atmospheric Research EDGAR (Janssens-Maenhout et al., 2017). The first  
74  $\Delta(^{14}\text{CO}_2)$  measurements in South Korea were reported by Turnbull et al. (2011a) based on air  
75 samples collected during October 2004 to March 2010 at Tae-Ahn Peninsula (TAP, 36.73° N,  
76 126.13° E, 20 m a.s.l.). This study showed that observed  $\text{CO}_2$  at this site was often influenced by  
77 Chinese emissions and the observed ratio of  $\Delta x(\text{CO}):C_{\text{ff}}$  ( $R_{\text{CO}}$ ) was greater than expected from  
78 bottom-up inventories. However South Korean  $\Delta(^{14}\text{CO}_2)$  data are still limited and the ratio of the  
79 other trace gases to  $C_{\text{ff}}$  barely discussed.

80 Here we use whole-air samples collected in glass flasks during May 2014 to August 2016 at  
81 Anmyeondo (AMY, 36.53° N, 126.32° E; 46 m a.s.l.) World Meteorological Organization  
82 (WMO) Global Atmosphere Watch (GAW) station, located on the west coast of South Korea and  
83 about 28 km SSE of TAP, where the first study was conducted. We decompose observed  $\text{CO}_2$   
84 enhancements into their fossil fuel and biological components at AMY to understand sources and  
85 sinks of  $\text{CO}_2$ . We also implemented cluster analysis using the NOAA Hybrid Single Particle  
86 Lagrangian Integrated Trajectory Model (HYSPLIT) to calculate back-trajectories for sample  
87 times and dates. Based on clusters of trajectories from specific regions, trace gas enhancement:  
88  $C_{\text{ff}}$  ratios and correlation coefficients were analyzed, especially focused on  $\text{SF}_6$  and  $\text{CO}$ , to  
89 determine the potential of alternative proxies to  $\Delta(^{14}\text{CO}_2)$ . Finally we compared our  $\Delta x(\text{CO}):C_{\text{ff}}$   
90 ratio with ratios determined from bottom-up inventories (EDGARv4.3.2) to evaluate reported  
91  $\text{CO}$  emissions and how they've changed since 2010.

## 92 **2. Materials and Method**

### 93 **2.1 Sampling site and methods**



94 The AMY GAW station is managed by the National Institute of Meteorological Sciences (NIMS)  
95 in the Korea Meteorological Administration (KMA). It has the longest record of continuous CO<sub>2</sub>  
96 measurement in South Korea, beginning in 1999. It is located on the west coast of Korea about  
97 130 km southwest of the megacity of Seoul, whose population was 9.8 million in 2017.  
98 Semiconductor and other industries exist within a 100 km radius of the station. Also, the largest  
99 thermal power plants fired by coal and heavy oil in South Korea are within 35 km to the  
100 northeast and southeast of the station. The closest town, around 30 km to the east of AMY, is  
101 well known for its livestock industries. Local economic activities are related to agriculture, e.g.,  
102 production of rice paddies, sweet potatoes, and onions, and the area is also known for its leisure  
103 opportunities that increase traffic and tourists in summer, indicating the complexity of  
104 greenhouse gas sources around AMY. On the other hand, air masses often arrive at AMY from  
105 the west and south, which is open to the Yellow Sea. Therefore AMY observes enhanced CO<sub>2</sub>  
106 compared to many other East Asian stations due not only to numerous local sources but also  
107 long-range transport of air-masses from the Asian continent (Lee et al., 2019).

108 Two pairs of flask-air samples (4 flasks total, 2 L, borosilicate glass with Teflon O-ring sealed  
109 stopcocks) were collected about weekly from a 40 m tall tower at AMY, regardless of wind  
110 direction and speed from May 2014 to August 2016, generally between 1400 to 1600 local time  
111 (Table S1). A total of 70 sets were collected and analyzed at the National Oceanic and  
112 Atmospheric Administration/Earth System Research Laboratory/Global Monitoring Division  
113 (NOAA/ESRL/GMD) for CO<sub>2</sub>, CO, and SF<sub>6</sub> and for  $\delta^{14}\text{C}$  by University of Colorado  
114 Boulder, Institute of Arctic and Alpine Research (INSTAAR). NOAA/ESRL/GMD analyzed  
115 CO<sub>2</sub> using a non-dispersive infrared analyzer, SF<sub>6</sub> using gas chromatography (GC) with electron  
116 capture detection, and CO by vacuum UV, resonance fluorescence. All analyzers were calibrated



117 with the appropriate WMO mole fraction scales (WMO-X2007 scale for CO<sub>2</sub>, WMO-X2014A  
118 scale for CO, and WMO-X2014 for SF<sub>6</sub>; <https://www.esrl.noaa.gov/gmd/ccl/>, last access: 4  
119 December 2019). The measurement and analysis methods for those gases are described in detail  
120 ([http://www.esrl.noaa.gov/gmd/ccgg/behind\\_the\\_scenes/measurementlab.html](http://www.esrl.noaa.gov/gmd/ccgg/behind_the_scenes/measurementlab.html), last access: 4  
121 December 2019). Measurement uncertainties for CO<sub>2</sub> and SF<sub>6</sub> are reported as 68% confidential  
122 intervals. For CO<sub>2</sub>, it is 0.07 μmol mol<sup>-1</sup> for all measurements used here. For SF<sub>6</sub>, it is 0.04 up to  
123 12 pmol mol<sup>-1</sup>, and undefined above that. For CO, measurement uncertainty has not yet been  
124 formally evaluated, but is estimated at 1 nmol mol<sup>-1</sup> (68% confidence interval). All CO<sub>2</sub>, SF<sub>6</sub> and  
125 CO data at AMY can be downloaded through [ftp://aftp.cmdl.noaa.gov/data/trace\\_gases/](ftp://aftp.cmdl.noaa.gov/data/trace_gases/).

126 The analysis methods for  $\Delta(^{14}\text{CO}_2)$  are described by Lehman et al.(2013). Measurement  
127 repeatability of  $\Delta(^{14}\text{CO}_2)$  in aliquots of whole air extracted from surveillance cylinders is 1.8‰  
128 ( $1\sigma$ ), roughly equating to 1 μmol mol<sup>-1</sup> C<sub>ff</sub> detection capability from the measurement  
129 uncertainty alone. The  $\Delta(^{14}\text{CO}_2)$  data at AMY was suggested in Table S1.

## 130 **2.2 Data analysis method using $\Delta(^{14}\text{CO}_2)$ data**

### 131 **2.2.1 Calculation of C<sub>ff</sub> and C<sub>bio</sub>**

132 As Turnbull et al. (2009) suggested the observed CO<sub>2</sub> (C<sub>obs</sub>) at AMY can be defined as:

$$133 \quad C_{\text{obs}} = C_{\text{bg}} + C_{\text{ff}} + C_{\text{other}} \quad (1)$$

134 where C<sub>bg</sub>, C<sub>ff</sub> and C<sub>other</sub> are the background, recently added fossil fuel CO<sub>2</sub> and the CO<sub>2</sub> derived  
135 from the other sources.



136 According to Tans et al. (1993), the product of CO<sub>2</sub> abundance and its isotopic ratio is conserved;  
137 the isotopic mass balance can be described as below:

$$138 \quad \Delta_{\text{obs}}C_{\text{obs}} = \Delta_{\text{bg}}C_{\text{bg}} + \Delta_{\text{ff}}C_{\text{ff}} + \Delta_{\text{other}}C_{\text{other}} \quad (2)$$

139 where  $\Delta$  is the  $\Delta^{14}\text{C}$  of each CO<sub>2</sub> component of Equ. (1).

140 Therefore we can calculate fossil fuel CO<sub>2</sub> by combining equations (1) and (2) as:

$$141 \quad C_{\text{ff}} = \frac{C_{\text{bg}}(\Delta_{\text{obs}} - \Delta_{\text{bg}})}{\Delta_{\text{ff}} - \Delta_{\text{bg}}} - \frac{C_{\text{other}}(\Delta_{\text{other}} - \Delta_{\text{bg}})}{\Delta_{\text{ff}} - \Delta_{\text{bg}}} \quad (3)$$

142 Fossil fuel derived CO<sub>2</sub> contains no <sup>14</sup>C because the half-life of <sup>14</sup>C is (5700±30) years (Godwin,  
143 1962) while these fuels are hundreds of millions of years old. As we mentioned in the section 1,  
144  $\Delta(^{14}\text{CO}_2)$  is reported as a per mil (‰) deviation from the absolute radiocarbon reference standard  
145 corrected for fractionation and decay with a simplified form;  $\Delta(^{14}\text{C})$   
146  $\approx [ (^{14}\text{C}/\text{C})_{\text{sample}} / (^{14}\text{C}/\text{C})_{\text{standard}} - 1 ] 1000\text{‰}$ . Therefore  $\Delta_{\text{ff}}$  is set at -1000‰ (Stuiver and  
147 Pollach, 1977). Background values ( $\Delta_{\text{bg}}$ ) in equations (1) to (3) are determined from  
148 measurements from background air collected at Niwot Ridge, Colorado, a high altitude site at a  
149 similar latitude as AMY (NWR, 40.05° N, 105.58° W, 3,526 m a.s.l.). Turnbull et al. (2011a)  
150 showed that the choice of background values did not significantly influence derived  
151 enhancements due to the large regional and local signal at TAP, 28 km from AMY. NWR  
152  $\Delta(^{14}\text{CO}_2)$  and other trace gas background values are selected using a flagging system to exclude  
153 polluted samples (Turnbull et al., 2007), and then fitted with a smooth curve following Thoning  
154 et al. (1989).



155 The second term of equation (3) is typically a small correction for the effect of other sources of  
156 CO<sub>2</sub> that have a  $\Delta^{14}\text{C}$  differing by a small amount that of the atmospheric background, such as  
157 CO<sub>2</sub> from 1) nuclear power industry, 2) oceans, 3) photosynthesis and 4) heterotrophic  
158 respiration.

159 1) The nuclear power industry produces  $^{14}\text{C}$  that can influence the  $C_{\text{ff}}$  calculation. South Korea  
160 has nuclear power plants along the east coast that may influence AMY air samples when air-  
161 masses originated from the eastern part of Korea (Figure 1). It is also possible that Chinese  
162 nuclear plants could influence some samples. Here we did not make any correction for this since  
163 most nuclear installations in this region are pressurized water reactors, which produce mainly  $^{14}\text{C}$   
164 in CH<sub>4</sub> rather than CO<sub>2</sub> (Graven and Gruber, 2011). 2) For the ocean, although there may also be  
165 a small contribution from oceanic carbon exchange across the Yellow Sea, we consider this  
166 effect small enough to ignore (Turnbull et al., 2011a). Larger scale ocean exchange and also  
167 stratospheric exchange affect both background and observed samples equally, so they can be  
168 ignored in the calculations. 3) For the photosynthetic terms,  $^{14}\text{C}$  in CO<sub>2</sub> accounts for natural  
169 fractionation during uptake, so we also set this observed value the same as the background value.  
170 4) Therefore we only consider heterotrophic respiration. For land regions, where most fossil fuel  
171 emissions occur, heterotrophic respiration could be a main contributor to the second term of  
172 equation (3) due to large  $^{14}\text{C}$  disequilibrium potentially. When this value is ignored,  $C_{\text{ff}}$  would be  
173 consistently underestimated (Palstra et al., 2008; Riley et al., 2008; Hsueh et al., 2007; Turnbull  
174 et al., 2006). For this, corrections were estimated as  $(-0.2 \pm 0.1) \mu\text{mol mol}^{-1}$  during winter and  $(-$   
175  $0.5 \pm 0.2) \mu\text{mol mol}^{-1}$  during summer (Turnbull et al., 2009; Turnbull et al., 2006).



176 CO<sub>2</sub> enhancements relative to baseline CO<sub>2</sub> are defined as  $\Delta x(\text{CO}_2)$ , with the excess signal of  
177  $C_{\text{obs}}$  minus  $C_{\text{bg}}$  in Equ.(1). Partitioning of  $\Delta x(\text{CO}_2)$  into  $C_{\text{ff}}$  and  $C_{\text{bio}}$  is calculated simply from the  
178 residual of the difference between observed  $\Delta x(\text{CO}_2)$  and  $C_{\text{ff}}$ .

### 179 **2.2.2 The ratio of trace gas enhancement to $C_{\text{ff}}$ and its correlation**

180 To obtain the correlation coefficient ( $r$ ) between  $C_{\text{ff}}$  and other trace gas enhancements ( $\Delta x(x) =$   
181  $x_{\text{obs}} - x_{\text{bg}}$ ) and the ratio of any trace gas to  $C_{\text{ff}}$  ( $R_{\text{gas}}$ ), we use reduced major axis (RMA) regression  
182 analysis. The distributions of  $R_{\text{gas}}$  are normally broad and non-Gaussian and RMA analysis is a  
183 relatively robust method of calculating the slope of two variables that show some causative  
184 relationship. Here,  $x_{\text{bg}}$  was derived from NWR with the same method described in section 2.2.1.

185 Therefore, the slope of the linear regression of the RMA fit can be expressed as

$$186 \quad R_{\text{gas}} = \sqrt{\frac{\sum \Delta x(x)^2 - (\sum \Delta x(x))^2/n}{\sum C_{\text{ff}}^2 - (\sum C_{\text{ff}})^2/n}} \quad (4)$$

187

188 And the uncertainty of  $R_{\text{gas}}$  is defined as

$$189 \quad U = \sqrt{\frac{\sum (\Delta x(x) - \Delta x(x)')^2/n}{\sum C_{\text{ff}}^2 - (\sum C_{\text{ff}})^2/n}} \quad (5)$$

190 Here,  $\Delta x(x)' = R_{\text{gas}} \times (C_{\text{ff}} - \overline{C_{\text{ff}}}) + \overline{\Delta x(x)}$

191

192 The correlation coefficient is expressed,



$$193 \quad r = \sqrt{\frac{(\sum \Delta x(x) C_{ff} - \frac{\sum \Delta x(x) \sum C_{ff}}{n})^2}{(\sum \Delta x(x)^2 - \frac{(\sum \Delta x(x))^2}{n}) \times (\sum C_{ff}^2 - \frac{(\sum C_{ff})^2}{n})}} \quad (6)$$

194 Results for each species are given in Table 1.

### 195 **2.3 HYSPLIT cluster analysis**

196 HYSPLIT trajectories were run using Unified Model-Global Data Assimilation and Prediction  
197 System (UM-GDAPS) weather data at 25 km by 25 km horizontal resolution to determine the  
198 regions that influence air mass transport to AMY. A total of 70 air-parcel back-trajectories were  
199 calculated for 72-h periods at 3-h intervals matching the time of each flask-air sample taken at  
200 AMY from May 2014 to August 2016. We assign the sampling altitude as 500 m, since it was  
201 demonstrated that HYSPLIT and other particle dispersion back-trajectory models (e.g.,  
202 FLEXPART) are consistent at 500 m altitude (Li et al., 2014). Cluster analysis of the resulting  
203 70 back-trajectories categorized six pathways through which air parcels arrive at AMY during  
204 the time period of interest.

205 Among the calculated back-trajectories, 67% indicate air masses originating from the Asian  
206 continent. Back-trajectories of continental background air (CB) originating in Russia and  
207 Mongolia occurred 13% of the time. 23% of the trajectories originated and travelled through  
208 northeast China (CN). The CN region includes Inner Mongolia and Liaoning, one of the most  
209 populated regions in China with 43.9 million people in 2012. These CN air masses arrive in  
210 South Korea after crossing through western North Korea. 17% of the trajectories are derived  
211 from central eastern China around the Shandong area (CE). The CE region contains Shandianzi  
212 (SDZ, 40.65° N, 117.12° E, 287 m a.s.l.) located next to the megacities of Beijing and Tianjin,  
213 which are some of China's highest CO<sub>2</sub> emitting regions (Gregg et al., 2008). 14% are Ocean



214 Background (OB) derived from the East China Sea, which passed over the eastern part of China  
215 such as Shanghai. Flow from South Korea also travels through heavily industrialized and/or  
216 metropolitan regions in South Korea (Korea Local, KL, 19%) and under stagnant conditions  
217 (Polluted Local region, PL, 14%). Some of the KL air-masses have also passed over the East Sea  
218 and Japan.

### 219 3. Results and discussions

#### 220 3.1 Observed $\Delta(^{14}\text{CO}_2)$ and portioning of $\text{CO}_2$ into $C_{\text{ff}}$ and $C_{\text{bio}}$

221 AMY  $\Delta(^{14}\text{CO}_2)$  values are almost always lower than those observed at NWR, which we consider  
222 to be broadly representative of background values for the mid-latitude Northern Hemisphere  
223 (Figure 2). NWR  $\Delta(^{14}\text{CO}_2)$ , which is based on weekly air samples, was in the range 10.0 to 21.2  
224 ‰, with an average  $(16.6 \pm 3)\%$  ( $1\sigma$ ) from May 2014 to August 2016. Waliguan (WLG, 36.28°  
225 N, 100.9° E, 3816 m a.s.l.), an Asian background GAW station in China, also showed similar  
226  $\Delta(^{14}\text{CO}_2)$  levels to NWR with an average of  $(17.1 \pm 6.8)\%$  in 2015 (Niu et al., 2016,  
227 measurement uncertainty  $\pm 3\%$ ).  $\Delta(^{14}\text{CO}_2)$  at AMY varied from -59.5 to 23.1‰ and had a mean  
228 value of  $(-6.2 \pm 18.8)\%$  ( $1\sigma$ ) during the experiment period (Table S1). This was similar to results  
229 from observations at SDZ, which is located about 100 km northeast of Beijing, in the range of -  
230 53.0 to 32.6‰ with an average  $(-6.8 \pm 21.1)\%$  during Sep 2014 to Dec 2015 (Niu et al., 2016).



231 Calculated  $C_{ff}$  at AMY ranges between  $-0.05$  and  $32.7 \mu\text{mol mol}^{-1}$  with an average of  $(9.7 \pm 7.8)$   
232  $\mu\text{mol mol}^{-1}$  ( $1\sigma$ ); high  $C_{ff}$  was observed regardless of season (Figure 2 (a)). One negative  $C_{ff}$   
233 value of  $-0.05 \mu\text{mol mol}^{-1}$  was estimated due to greater AMY  $\Delta(^{14}\text{CO}_2)$  than NWR on July 30,  
234 2014. Although negative  $C_{ff}$  values are non-physical, this value is not significantly different from  
235 zero, and is reasonable given that this air originated from the OB sector. The range of  $C_{ff}$  in the  
236 AMY samples is similar to that observed at TAP from 2004 to 2010 ( $-1.6$  to  $42.9 \mu\text{mol mol}^{-1}$   
237  $C_{ff}$ ), but  $C_{ff}$  is on average about twice as high at AMY as in the 2004 to 2010 TAP samples  
238 (mean  $(4.4 \pm 5.7) \mu\text{mol mol}^{-1}$ ) (Turnbull et al., 2011a). A more detailed comparison of results  
239 based on differences between samples derived from the Asian continent and Korea local air is  
240 provided in section 3.2.

241 Estimated  $C_{bio}$ , as defined in section 2.2.1, varied from  $-18.1$  to  $15.7 \mu\text{mol mol}^{-1}$  (mean  $(0.9 \pm 5.8)$   
242  $\mu\text{mol mol}^{-1}$ ) at AMY (Figure 2 (c)).  $C_{bio}$  showed a strong seasonal cycle with the lowest values  
243 from July to September when photosynthetic drawdown is expected to be strongest, in good  
244 agreement with the previous TAP study (Turnbull et al., 2011a). Even though  $C_{bio}$  was at times  
245 negative, mainly due to photosynthesis during summer, the largest positive  $C_{bio}$  was also  
246 observed in summer.

247 The largest  $C_{ff}$  by season was observed in order of winter (DJF,  $(11.3 \pm 7.6)$ ,  $n=14$ ) > summer  
248 (JJA,  $(10.7 \pm 9.2)$ ,  $n=11$ ) > spring (MAM,  $(8.6 \pm 8.0)$ ,  $n=22$ ) > autumn (SON,  $(7.6 \pm 5.6)$ ,  $n=17$ ) with  
249 a unit of  $\mu\text{mol mol}^{-1}$ . When we consider only positive contributions of  $C_{bio}$  samples, the order  
250 was summer  $((4.6 \pm 4.0)$ ,  $n=14$ ) > autumn  $((4.1 \pm 2.5)$ ,  $n=9$ ) > spring  $((3.8 \pm 2.6)$ ,  $n=13$ ) > winter  
251  $((3.4 \pm 2.5)$ ,  $n=11$ ) with a unit of  $\mu\text{mol mol}^{-1}$ .



252  $C_{ff}$  in summer was nearly as high as in winter. This is because lower wind speeds are observed at  
253 AMY during summer (Lee et al., 2019), suggesting that these summer high values may reflect  
254 emission from local activities, which were described in section 2.1, more than in other seasons.  
255 The highest  $C_{bio}$  value was also observed in summer. PL sector showed that positive  $C_{bio}$   
256 correlates with  $CH_4$ , which is a tracer for agriculture when observed in TAP local air masses.  
257 Turnbull et al.(2011a) also showed similar results.

258 In winter,  $C_{bio}$  was relatively lower than in other seasons while  $C_{ff}$  was highest. During winter,  
259 AMY is mainly affected by long-range transport of air-masses from China due to the Siberian  
260 high (Lee et al., 2019). Therefore air samples were less affected by local activities in winter but  
261  $C_{bio}$  still contributed almost 23% to  $\Delta x(CO_2)$ . In the dry season (from October to March), forest  
262 fires, which contribute the largest portion of total  $CO_2$  emissions from open fires at the national  
263 scale, are concentrated in northeastern and southern China (Yin et al., 2019). The highest CO  
264 was observed in winter ( $(449.1 \pm 244.1)$  nmol mol<sup>-1</sup> ( $1\sigma$ ) in winter while ( $236.8 \pm 124.4$ ) nmol  
265 mol<sup>-1</sup> ( $1\sigma$ ) in summer), which also supports biomass burning and bio fuels as large contributors  
266 to observed  $CO_2$  enhancements in winter. Turnbull et al. (2011a) also showed that 20-30% of  
267 winter  $CO_2$  enhancements at TAP were likely contributed by biofuel combustion, along with  
268 plant, soil, human, and animal respiration.

269 Regardless of the source, we find that  $C_{bio}$  contributes substantially to atmospheric  $CO_2$   
270 enhancements at AMY in air masses affected by local and long-range transport, so  $CO_2$   
271 enhancements above background cannot be reliably interpreted as entirely due to  $C_{ff}$ .

272 **3.2  $C_{ff}$  comparison between Korea Local and Asian Continent samples**



273 To more clearly identify samples originating from the Asian continent (trajectory clusters CB,  
274 CN, CE, and OB) and Korea Local (trajectory cluster KL) after cluster analysis of the 70 sets of  
275 measurements, we use wind speed data from the Automatic Weather System (AWS) installed at  
276 the same level as the air sample inlet at AMY. Among the data from CB, CN, CE, OB, and KL,  
277 when wind speed was less than 3 m/s, we assumed that those samples could be affected by local  
278 pollution. PL was also ruled out since it was affected by local pollutions under the stagnant  
279 condition. Therefore we use only 41 sets of observations for this analysis (Table 1).

280  $C_{ff}$  is highest in the order  $CE > CN > KL > CB > OB$  (Table 1). During the experimental period,  
281 the averages from Asian continent (sectors CE and CN) were higher than KL without the  
282 baseline level. The calculated mean  $C_{ff}$  using only CE, CN, CB and OB, which sample  
283 substantial outflow from the Asian Continent, was  $(7.6 \pm 3.9) \mu\text{mol mol}^{-1}$ .

284 When we compared the KL samples  $((8.6 \pm 5.3) \mu\text{mol mol}^{-1})$  with those from Korea Local air-  
285 masses observed at TAP  $((8.5 \pm 8.6) \mu\text{mol mol}^{-1}$ , Turnbull et al., 2011a), mean  $C_{ff}$  was quite  
286 similar (Figure 3). However, when comparing the  $C_{ff}$  values from CB air masses in this study  
287 and TAP far-field (from China) samples (Turnbull et al., 2011a),  $C_{ff}$  almost doubled from  $(2.6 \pm$   
288  $2.4)$  to  $(4.3 \pm 2.1) \mu\text{mol mol}^{-1}$ , even though they might be expected to have had similar air mass  
289 back-trajectories. We also compared the values at SDZ from 2009 to 2010 (Turnbull et al., 2011a)  
290 and in 2015 (Niu et al., 2016); they also increased, not only in the samples that were affected by  
291 Beijing and North China Plain (SDZ-BN), which are comparably polluted, but also in the  
292 samples that were affected by northeast China (SDZ-NE). For SDZ-BN samples,  $C_{ff}$  increased



293 from  $(10 \pm 1)$  to  $(16 \pm 7.6)$   $\mu\text{mol mol}^{-1}$  from 2009/2010 to 2015. The AMY samples from CE,  
294 which flow over Beijing, showed  $(11.2 \pm 8.3)$   $\mu\text{mol mol}^{-1}$  of  $C_{\text{ff}}$  and were also slightly greater  
295 than the 2009 – 2010 SDZ-BN samples (Turnbull et al., 2011a). For SDZ-NE samples,  $C_{\text{ff}}$  was  
296  $(3 \pm 7)$   $\mu\text{mol mol}^{-1}$  in 2009 to 2010 and increased to  $(7.6 \pm 6.8)$   $\mu\text{mol mol}^{-1}$  in 2015. Since the  
297 SDZ-NE samples are affected by northeast China according to Turnbull et al. (2011a) and Niu et  
298 al. (2016), we also see CN originated from northeast China and it was around  $(10.6 \pm 6.9)$   $\mu\text{mol}$   
299  $\text{mol}^{-1}$ .

300 It has been suggested that inter-annual variability in observed mean  $C_{\text{ff}}$  in South Korea could  
301 reflect changing fossil fuel  $\text{CO}_2$  emissions, or could indicate inter-annual variability in the air  
302 mass trajectories of the (small) dataset of flask-air samples (Turnbull et al., 2011a). Even though  
303 the growth rate of  $C_{\text{ff}}$  emission has been decreasing slowly in East Asia since 2010 due to  
304 emission reduction policies (Labzovskii et al., 2019), reported emissions increased 16.7% in  
305 China and 1.8% in South Korea from 2010 to 2016 (Janssens-Maenhout et al., 2017). This is  
306 broadly consistent with the flat trend in observed  $C_{\text{ff}}$  in Korea Local air masses, and in the  
307 upward trend in  $C_{\text{ff}}$  observed in air-masses flowing out from Asia. Therefore it is possible that  
308 AMY mean  $C_{\text{ff}}$  increased relative to the earlier TAP observations due to increased fossil fuel  
309 emissions from the Asian continent. It is also likely that the proximity of local emission sources  
310 to AMY is causing higher observed  $C_{\text{ff}}$  under some synoptic conditions.

311 On the other hand, those values from this study showed large variability with small sample  
312 numbers, further study will be necessary.



### 313 3.3. Correlation of $C_{ff}$ with $SF_6$ and CO, and their emission ratios

314 We calculated correlation coefficients ( $r$  from Equ. (6)) between  $SF_6$  and CO enhancements with  
315  $C_{ff}$  and their ratios from Equ. (4) with the 50 samples that were described in section 3.2 including  
316 PL sector ( $n=9$ ) and whose values are tabulated in Table 1.

317 The correlations of CO enhancements ( $\Delta x(CO)$ ) with  $C_{ff}$  were strong ( $r > 0.7$ ) in all sectors  
318 except PL, while  $SF_6$  enhancements ( $\Delta x(SF_6)$ ) correlated strongly with  $C_{ff}$  ( $r > 0.8$ ) for CE and  
319 OB in outflow from the Asian Continent and KL.  $R_{CO}$  and  $R_{SF_6}$  were different between Korea  
320 Local and outflows from the Asian Continent.

321 For  $SF_6$ , observed mean levels were high in order of  $KL > PL > CN$  and  $CE > OB > CB$  (Table  
322 1).  $SF_6$  in KL and PL were higher than from the Asian Continent, since South Korea has larger  
323  $SF_6$  emissions than most countries (ranked at 4<sup>th</sup> as of 2010 according to the EDGAR4.2.)  
324 because of liquid-crystal display (LCD) and electrical equipment production (Fang et al., 2014).  
325 Even though South Korea showed higher  $SF_6$ , the correlation is different between KL and PL.  
326 Under stagnant conditions, emitted  $SF_6$  is less diluted by mixing, so that in PL,  $\Delta x(SF_6)$   
327 correlated weakly with  $C_{ff}$ . On the other hand, KL, CE and OB showed strong correlations ( $r >$   
328 0.8). Those three sectors are also larger  $SF_6$  sources compared to other regions, according to  $SF_6$   
329 emission estimates for Asia (Fang et al., 2014). Because long-range transport allows time for  
330 mixing,  $SF_6$  and  $C_{ff}$  emissions are effectively co-located at not only continental scales but also  
331 regional scales. Thus  $SF_6$  can be a good tracer of fossil fuel  $CO_2$ .

332 Even though the correlation between  $\Delta x(SF_6)$  and  $C_{ff}$  was strong in CE, OB and KL,  $R_{SF_6}$  is  
333 different between South Korea and outflow from the Asian continent (Figure S2). In a previous  
334 study, observed  $R_{SF_6}$  was 0.02 to 0.03  $pmol \mu mol^{-1}$  at NWR in 2004 (Turnbull et al., 2006). Here,



335 the ratio was at  $(0.19 \pm 0.03)$  and  $(0.17 \pm 0.03)$   $\text{pmol } \mu\text{mol}^{-1}$  for CE and OB respectively. For KL,  
336 it was  $(0.66 \pm 0.16)$   $\text{pmol } \mu\text{mol}^{-1}$  indicating much larger ratios than in outflow from the Asian  
337 continent. Further, observed  $R_{\text{SF}_6}$  is 2 to 3 times greater for all air masses than predicted from  
338 bottom-up inventories based on national scale roughly. For this calculation, we use EDGAR4.3.2  
339 for  $\text{CO}_2$  and EDGAR4.2 for  $\text{SF}_6$ . We repeat the calculations for both  $\text{CO}_2$  and  $\text{SF}_6$  with Korea's  
340 National Inventory Report (KNIR, Greenhouse Gas Inventory and Research Center, 2018).  
341 Using  $\text{SF}_6$  for 2010 from EDGAR4.2, we obtain  $R_{\text{SF}_6}$  of  $0.08 \text{ pmol } \mu\text{mol}^{-1}$  for China while for  
342 South Korea it was  $0.14 \text{ pmol } \mu\text{mol}^{-1}$ . Especially for South Korea, this is much lower than the  
343 observed  $R_{\text{SF}_6}$ . When KL  $R_{\text{SF}_6}$  was compared to ratios calculated from the KNIR inventory ( $0.27$   
344  $\text{pmol } \mu\text{mol}^{-1}$  for 2010 and  $0.22 \text{ pmol } \mu\text{mol}^{-1}$  for 2014), it was closer to observed  $R_{\text{SF}_6}$  than  
345 EDGAR, but still underestimated (Figure S3 and S2). This result suggests that the observed ratio  
346 could be used to re-evaluate the bottom-up inventories (Rivier et al., 2006), especially targeting  
347 the Asian continent. Since KL  $R_{\text{SF}_6}$  showed greater uncertainty than CE and OB, it would be  
348 useful to get more data to try and derive a more robust estimate to evaluate  $\text{SF}_6$  emissions in  
349 Korea.

350 High CO was mainly observed in outflow from the Asian continent in order of  $\text{CE} > \text{CN} > \text{PL} >$   
351  $\text{CB} > \text{KL} > \text{OB}$  (Table 1). The order of CO is quite different to that of  $\text{SF}_6$ . CO from KL and PL  
352 is lower than from outflow from the Asian continent, except for the OB sector, indicating that  
353 high CO can be a tracer of outflow from the Asian continent. Since CO is produced during  
354 incomplete combustion, it is more closely related to fossil fuel  $\text{CO}_2$  emissions than the other  
355 trace gases. Therefore in most cases the correlation between CO and  $C_{\text{ff}}$  was strong.  $R_{\text{CO}}$  was  
356 very different between air masses originating from South Korea Local ( $(8 \pm 2) \text{ nmol } \mu\text{mol}^{-1}$ ) and



357 the Asian continent ( $(29 \pm 8)$  to  $(36 \pm 2)$   $\text{nmol } \mu\text{mol}^{-1}$ ), likely due to differences in combustion  
358 efficiencies. The higher continental emission ratios may also result from some contribution of  
359 biofuel combustion and agricultural burning in the Asian continent, which have significantly  
360 higher CO emission than fossil-fuel combustion (Akagi et al., 2011).

361 Typically CO shows seasonal variations with lower values in summer due to the photochemical  
362 sink. Among the samples, the samples collected in summer were mainly rejected through wind  
363 speed cut-off (less than 3 m/s) since AMY has lower wind speed in summer (Lee et al., 2019).  
364 Only OB sector includes 4 summer samples (of 7), because summer air masses are mainly from  
365 the southern part of the Yellow Sea (Lee et al., 2019). However, we assumed  $R_{\text{CO}}$  is less affected  
366 by the summer sink, since only two  $\Delta x(\text{CO})$  samples were negative for OB (Figure S2) and  $R_{\text{CO}}$   
367 was consistent whether or not the negative  $\Delta x(\text{CO})$  values were considered. We compare our  $R_{\text{CO}}$   
368 to results from previous studies in section 3.4.

### 369 **3.4 Comparison of measured emission ratios to CO inventory data**

370 To compare emission ratios derived from atmospheric observations with those from inventories  
371 for 2000 to 2012, we calculated inventory emission ratio ( $I_{\text{CO}/\text{CO}_2}$ ) as:

$$372 \quad I_{\text{CO}/\text{CO}_2} = E_{\text{CO}}/E_{\text{CO}_2} \times M_{\text{CO}_2}/M_{\text{CO}} \quad (7)$$

373 Where,  $E_{\text{CO}}$  and  $E_{\text{CO}_2}$  are total CO and fossil fuel  $\text{CO}_2$  emissions in gigagrams (Gg,  $10^9$  g) from  
374 the bottom-up national inventory.  $M_X$  are the molar masses of CO and  $\text{CO}_2$  in  $\text{g mol}^{-1}$ .

375 We use EDGAR4.3.2 (Janssens-Maenhout et al., 2017) and KNIR (Greenhouse Gas Inventory  
376 and Research Center, 2018) for inventory information for both CO and  $\text{CO}_2$ .



377 The uncertainty of EDGAR4.3.2 emissions was reported as a 95% confidence interval (Janssens-  
378 Maenhout et al., 2019),  $\pm 5.4\%$  for China and  $\pm 3.6\%$  for South Korea (personal communication  
379 with Dr. Efisio Solazzo). The uncertainties of CO and SF<sub>6</sub> emissions were not reported by  
380 EDGAR. For KNIR, the CO<sub>2</sub> 2016 emission uncertainty in the energy sector was  $\pm 3\%$   
381 (Greenhouse Gas Inventory and Research Center, 2018). KNIR does not provide uncertainties  
382 for other emission sectors of CO<sub>2</sub>, nor from emissions of CO and SF<sub>6</sub>.

383 In Fig. 4 we confirm that the CO to C<sub>ff</sub> emission ratios ( $R_{CO}$ ) derived from both observations and  
384 inventories for China and South Korea are decreasing. Since C<sub>ff</sub> emissions appear to be flat  
385 (South Korea) or slightly increasing (China), this indicates that combustion efficiency and/or  
386 scrubbing of CO is improving.

387 For South Korea, EDGAR4.3.2 indicated that CO emissions from the energy sector (98% to 99%  
388 of total emission) decreased by 47% between the 1997 and 2012. South Korean fossil fuel CO<sub>2</sub>  
389 emissions increased until 2011 and remained mostly constant from 2011 to 2016  
390 ((603,901 $\pm$ 4,315) Gg CO<sub>2</sub>) (Figure S4). Therefore the decreased trend in the emission ratio  
391 seems to reflect recent decreases in CO emissions in South Korea. Turnbull et al. (2011a)  
392 determined an observed mean  $R_{CO}$  of (13 $\pm$ 3) nmol  $\mu\text{mol}^{-1}$  during 2004 to 2010. Suntharalingam  
393 et al. (2004) estimated  $R_{CO}$  15.4 nmol  $\mu\text{mol}^{-1}$  for South Korea in 2001 from CO<sub>2</sub> and CO airborne  
394 observations (C<sub>ff</sub> was not determined). Recently, the KORUS-AQ campaign, which was  
395 conducted over Seoul from May to June in 2016, estimated  $R_{CO}$  as 9 nmol  $\mu\text{mol}^{-1}$  (Tang et al.,  
396 2018) based on CO<sub>2</sub> and CO observations (C<sub>ff</sub> was not determined). Our study gives  $R_{CO}$  of (8 $\pm$ 2)



397  $\text{nmol } \mu\text{mol}^{-1}$  for South Korea, slightly but not significantly lower than the KORUS-AQ result for  
398 Seoul. This difference could be due to different source regions (Seoul vs the larger Korean  
399 region) and different experimental periods (two months vs two years). Different contributions of  
400  $C_{\text{bio}}$  and  $C_{\text{ff}}$  to total  $\text{CO}_2$  may bias the  $R_{\text{CO}}$  calculation when total  $\text{CO}_2$  was used in the KORUS-  
401 AQ study (e.g., Miller et al., 2012). The South Korean national  $R_{\text{CO}}$  from EDGAR4.3.2 in 2012  
402 was  $6.7 \text{ nmol } \mu\text{mol}^{-1}$ , consistent with our observations. Using KNIR for 2016, we obtain  $R_{\text{CO}}$  of  
403  $2.1 \text{ nmol } \mu\text{mol}^{-1}$ . KNIR seems to have uncounted CO emissions, since it is unreasonably low  
404 during all comparison periods (Figure S5). For example, CO emissions recently derived from  
405 fugitive emissions and residential/other sectors increased to 14% and 11.5% of total emission  
406 respectively in EDGAR but were not reported in KNIR.

407 For China the inventories estimate that CO emissions from the energy sector,  $(96.5 \pm 0.2)\%$ , were  
408 almost constant through the 1990s, and then increased during the early-2000s from industrial  
409 processes (8.8% of total emissions in 2012). Fossil fuel  $\text{CO}_2$  emission in China also increased  
410 until 2013 and then stayed roughly constant at  $(10,461,890 \pm 60,571) \text{ Gg}$  according to  
411 EDGAR4.3.2. Thus even though both emissions show an increase from 2000 to 2016 for fossil  
412 fuel  $\text{CO}_2$  and to 2012 for CO, the emission ratio decreased (Figure S4 and Figure 4) seeming to  
413 indicate that combustion efficiency is improving. Many studies observed decreasing  $R_{\text{CO}}$  in  
414 China from 2000 to 2010 (Turnbull et al., 2011a; Wang et al., 2010). Suntharalingam et al. (2004)  
415 reported  $R_{\text{CO}}$  was  $55 \text{ nmol } \mu\text{mol}^{-1}$  in 2001 ( $C_{\text{ff}}$  was not determined). In the Beijing region,  $R_{\text{CO}}$   
416 decreased from 57.80 to  $37.59 \text{ nmol } \mu\text{mol}^{-1}$  during 2004 to 2008 (Wang et al., 2010). The overall  
417  $R_{\text{CO}}$  was  $(47 \pm 2) \text{ nmol } \mu\text{mol}^{-1}$  at SDZ for 2009-2010 and  $(44 \pm 3) \text{ nmol } \mu\text{mol}^{-1}$  in air-masses that  
418 originated from the Asian continent from 2005 to 2009 (Turnbull et al., 2011a). Tohjima et al.



419 (2014) explained that surface based  $R_{CO}$  decreased from 45 to 30  $\text{nmol } \mu\text{mol}^{-1}$  in outflow air  
420 masses from China from 1998 to 2010. Fu et al. (2015) also observed  $R_{CO}$  of 29  $\text{nmol } \mu\text{mol}^{-1}$   
421 over mainland China in 2009. In Beijing, which is located along the path of CE, it was  $(30.4 \pm 1.6)$   
422  $\text{nmol } \mu\text{mol}^{-1}$  and  $(29.6 \pm 3.2)$   $\text{nmol } \mu\text{mol}^{-1}$  for Xiamen in 2016, which is in the OB sector (Niu et  
423 al., 2018). During KORUS-AQ in 2016,  $R_{CO}$  of 28  $\text{nmol } \mu\text{mol}^{-1}$  was observed over the Yellow  
424 Sea. Some of those studies did not differentiate  $C_{fr}$  from the total  $\text{CO}_2$  enhancement, so, although  
425  $R_{CO}$  still includes uncertainties, it is continually decreasing.

426 In this study  $R_{CO}$  is  $(29 \pm 8)$ ,  $(31 \pm 8)$ ,  $(36 \pm 2)$ , and  $(31 \pm 4)$   $\text{nmol } \mu\text{mol}^{-1}$  for CB, CN, CE and OB,  
427 consistent with Tang et al.(2018) and Liu et al.(2018). On the other hand,  $R_{CO}$  in CE is higher  
428 than in other sectors in this study. The Shandong area, which is located in the path of CE, has  
429 been plagued with problems of combustion inefficiency and ranked as the largest consumer of  
430 fossil fuels in all of China (Chen and Li, 2009). The uncertainties in our observed  $R_{CO}$  for this  
431 region overlap with other sectors such as CB, CN and OB, so further monitoring of the ratios  
432 will help to get more detailed information.

433 In South Korea and China, atmosphere-based  $R_{CO}$  values are 1.2 times and  $(1.8 \pm 0.2)$  times  
434 greater than in the inventory, respectively. This is in agreement with previous studies (Turnbull  
435 et al., 2011a; Kurokawa et al., 2013; Tohjima et al., 2014). One explanation is that EDGAR does  
436 not reflect secondary CO production, which can be a significant contributor to CO (Kurokawa et  
437 al., 2013). Also, CO derived from biomass burning and biofuels was not included in this  
438 inventory. Therefore, this indicates that top-down observations are necessary to evaluate and  
439 improve bottom-up emission products.



#### 440 4. Summary and conclusion

441 Observed  $\Delta(^{14}\text{CO}_2)$  values at AMY ranged from -59.5 to 23.1‰ (a mean value of  $(-6.2 \pm 18.8)$   
442 ‰ ( $1\sigma$ )) during the study period, almost always lower than those observed at NWR, which we  
443 consider to be broadly representative of background values for the mid-latitude Northern  
444 Hemisphere. This reflects the strong imprint of fossil fuel- $\text{CO}_2$  emissions recorded in AMY air  
445 samples. Calculated  $C_{\text{ff}}$  using  $\Delta(^{14}\text{CO}_2)$  at AMY ranges between -0.05 and  $32.7 \mu\text{mol mol}^{-1}$  with  
446 an average of  $(9.7 \pm 7.8) \mu\text{mol mol}^{-1}$  ( $1\sigma$ ); this average is twice as high as in the 2004 to 2010  
447 TAP samples (mean  $(4.4 \pm 5.7) \mu\text{mol mol}^{-1}$ ) (Turnbull et al., 2011a). We also observed high  $C_{\text{ff}}$   
448 regardless of the season or source region. After separately identifying samples originating from  
449 the Asian continent and the Korean peninsula, we determined that the mean  $C_{\text{ff}}$  increased relative  
450 to the earlier observations due to increased fossil fuel emissions from the Asian continent. Note,  
451 however, that our data span a relatively limited time period, so a longer time-series would  
452 increase confidence in tracking this change.

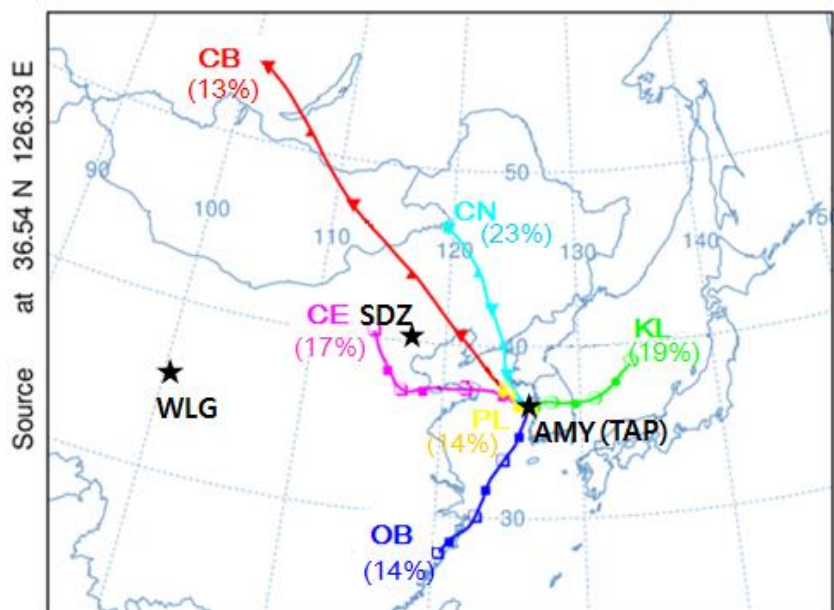
453 Because  $\Delta x(\text{CO})$  and  $\Delta x(\text{SF}_6)$  agreed well with  $C_{\text{ff}}$ , but showed different slopes for Korea and the  
454 Asian continent, those  $R_{\text{gas}}$  values can be indicators of air mass origin and those gases can be  
455 proxies for  $C_{\text{ff}}$ . Overall, we have confirmed that both  $R_{\text{CO}}$  derived from inventory and  
456 observation have decreased relative to previous studies, indicating that combustion efficiency is  
457 increasing in both China and South Korea. Atmosphere-based  $R_{\text{CO}}$  values are 1.2 times and  
458  $(1.8 \pm 0.2)$  times greater than in inventory values for South Korea and China, respectively. This  
459 discrepancy may arise from several sources including the absence of atmospheric chemical CO



460 production such as oxidation of  $\text{CH}_4$  and non-methane VOCs. Therefore those values can be  
461 used for improving bottom-up inventory in the future. Finally, we stress that because  $C_{\text{bio}}$   
462 contributes substantially to  $\Delta x(\text{CO}_2)$ , even in winter,  $\Delta^{14}\text{C}$ -based  $C_{\text{ff}}$  (and not  $\Delta x(\text{CO}_2)$ ) is  
463 required for accurate calculation of both  $R_{\text{CO}}$  and  $R_{\text{SF}_6}$ .



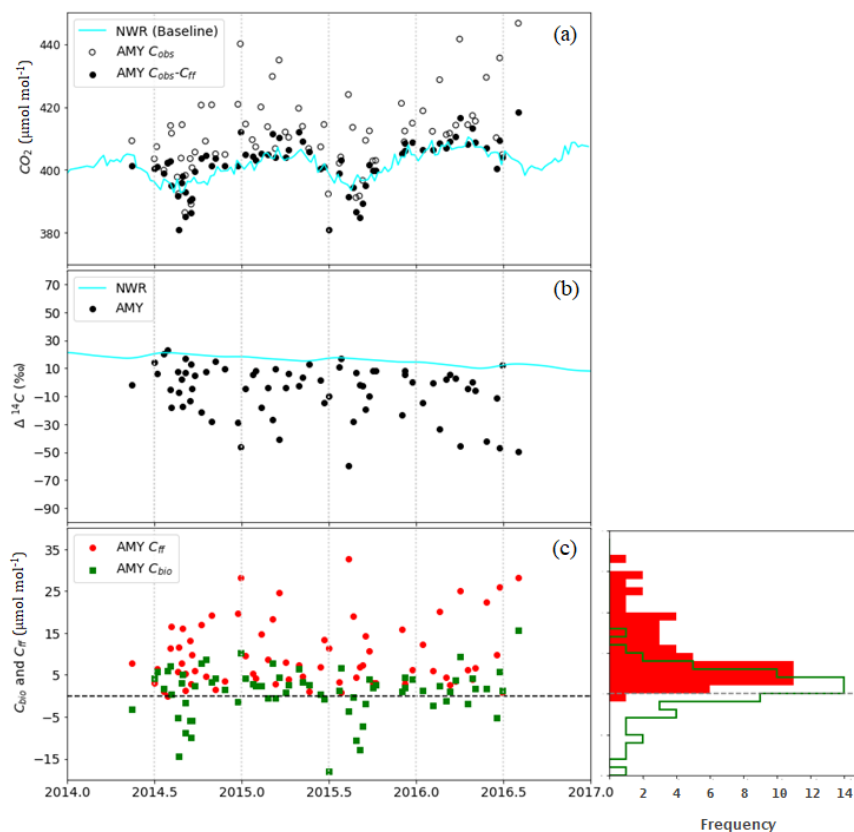
464



465

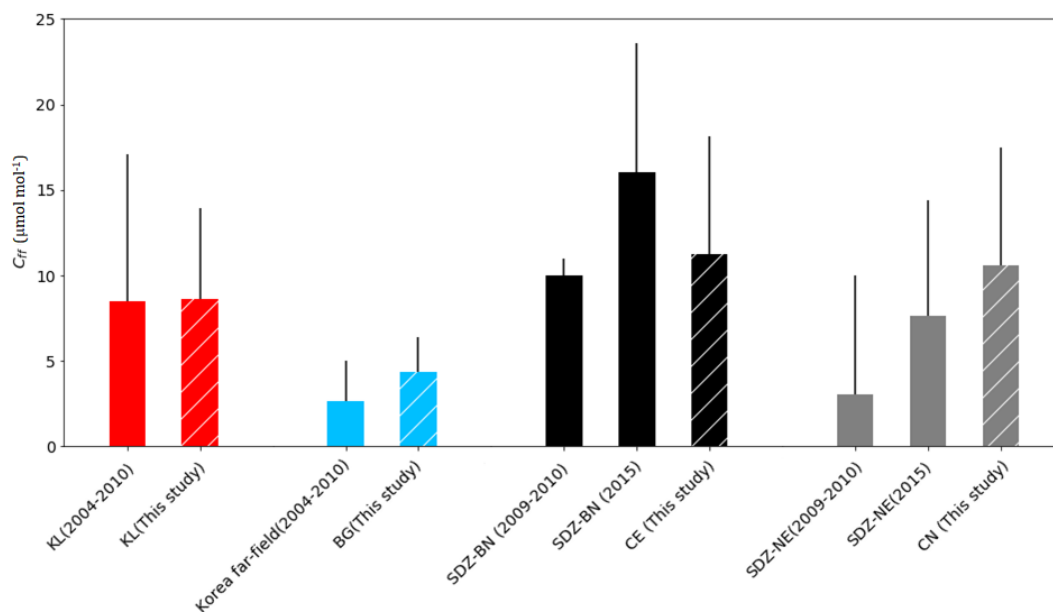
466 Figure 1. A total of 70 air-parcel back-trajectories were calculated for 72-h periods at 3-h  
467 intervals from May 2014 to August 2016 using the HYSPLIT model in conjunction with KMA  
468 UM GDAPS data at 25 km by 25 km resolution. Station locations are: WLG (Waliguan, 36.28°  
469 N, 100.9° E, 3816 m a.s.l.), SDZ (Shandianzi, 40.65° N, 117.12° E, 287 m a.s.l.), and AMY  
470 (Anmyeondo, 36.53° N, 126.32° E, 86 m a.s.l.). TAP (Tae-Ahn Peninsula, 36.73° N, 126.13° E,  
471 20 m a.s.l.) is around 28 km northeast from AMY.

472



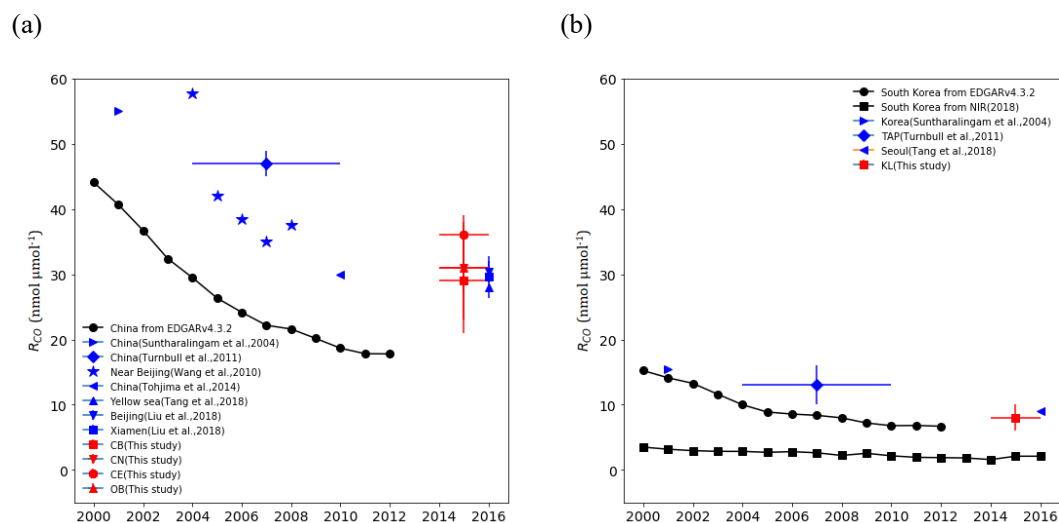
473  
474 Figure 2. Time series of (a) observed CO<sub>2</sub> dry air mole fraction (open circles) and observed CO<sub>2</sub>  
475 (C<sub>obs</sub>) minus C<sub>ff</sub> calculated from Δ(<sup>14</sup>CO<sub>2</sub>) (closed circles). (b) Δ(<sup>14</sup>CO<sub>2</sub>) at AMY (black circles)  
476 and at NWR (Niwt Ridge, line), baseline data. (c) Time series of C<sub>ff</sub> and C<sub>bio</sub> calculated from  
477 Δ(<sup>14</sup>CO<sub>2</sub>) at AMY.

478



479

480 Figure 3. Calculated  $C_{fr}$  ( $\mu\text{mol mol}^{-1}$ ). Red bars are for KL and blue bars are for Korea far-field  
481 (China) (2004-2010 from Turnbull et al. (2011a)). Black bars are for SDZ-BN samples that were  
482 affected by Beijing and North China plain. Gray bars for SDZ-NE indicate samples that were  
483 affected by regions northeast of SDZ. SDZ (2009-2010) is from Turnbull et al. (2011a) and SDZ  
484 (2015) is from Niu et al. (2016). Hatched red, blue, black and grey bars are derived from this  
485 study during 2014 to 2016.



486 Figure 4.  $R_{CO}$  for China (a) and for South Korea (b). Black circles: EDGARv.4.3.2 emission  
487 inventory. Black squares: National Inventory Report, Korea (2018). Blue symbols are from other  
488 studies (Suntharalingam et al., 2004; Wang et al., 2010; Turnbull et al., 2011a; Tohjima et al.,  
489 2014; Liu et al., 2018; Tang et al., 2018). Red symbols: This study. Y-error bars: uncertainty  
490 according to equation (5). X-error bars: the period for the mean value.

491



492 Table 1. Means and standard deviations of  $C_{\text{ff}}$  ( $\mu\text{mol mol}^{-1}$ ), CO ( $\text{nmol mol}^{-1}$ ) and SF<sub>6</sub> ( $\mu\text{mol}$   
493  $\text{mol}^{-1}$ ) (total N=50, without PL N=41). The correlations ( $r$ ) and the ratio ( $R_{\text{gas}}$ ) of enhancement  
494 between  $C_{\text{ff}}$  were determined by Reduced Major Axis (RMA) regression analysis on each scatter  
495 plot to obtain regression slopes. The uncertainty of  $R_{\text{gas}}$  refers to equation (5). When  $r$  is less than  
496 0.7,  $R_{\text{gas}}$  was not included here. N is the number of data. The unit of  $R_{\text{CO}}$  is  $\text{nmol } \mu\text{mol}^{-1}$  and for  
497  $R_{\text{SF}_6}$  it is  $\text{pmol } \mu\text{mol}^{-1}$ . A plot of  $R_{\text{CO}}$  and  $R_{\text{SF}_6}$  is shown in Figure S1.

|                              | Outflow from the Asia continent |                |                     |                     | South Korea         |             |
|------------------------------|---------------------------------|----------------|---------------------|---------------------|---------------------|-------------|
|                              | CB (N=7)                        | CN (N=9)       | CE (N=9)            | OB (N=7)            | KL (N=9)            | PL (N=9)    |
| $C_{\text{ff}}$              | 4.3±2.1                         | 10.6±6.9       | 11.2±8.3            | 4.1±2.7             | 8.6±5.3             | 15.6±11.6   |
| CO                           | 233±59                          | 353±219        | 473±293             | 169±90              | 228±40              | 259±100     |
| SF <sub>6</sub>              | 9.0±0.4                         | 10.1±1.2       | 10.1±1.5            | 9.2±0.5             | 13.0±3.3            | 12.7±6.2    |
| $R_{\text{CO}}$<br>( $r$ )   | 29±8<br>(0.80)                  | 31±8<br>(0.76) | 36±2<br>(0.98)      | 31±4<br>(0.96)      | 8±2<br>(0.74)       | -<br>(0.44) |
| $R_{\text{SF}_6}$<br>( $r$ ) | -<br>(0.63)                     | -<br>(0.48)    | 0.19±0.03<br>(0.91) | 0.17±0.03<br>(0.94) | 0.66±0.16<br>(0.76) | -<br>(0.38) |

498  
499



500 **Data availability**

501  
502 Our CO<sub>2</sub>, CO, SF<sub>6</sub> data from AMY and NWR can be downloaded from  
503 [ftp://aftp.cmdl.noaa.gov/data/trace\\_gases](ftp://aftp.cmdl.noaa.gov/data/trace_gases).  $\Delta(^{14}\text{CO}_2)$  data are provided in the supplementary  
504 material of this paper.

505

506 **Author contributions**

507 HL wrote this paper and analyzed all data. HL and GWL designed this study. EJD and JCT  
508 guided and reviewed this paper. SL collected samples and gave the information of the data at  
509 AMY. EJD, JCT, SJL, JBM, GP, and JL provided data and reviewed the manuscript. SSL and  
510 YSP reviewed this paper. All authors contributed this work.

511

512 **ACKNOWLEDGMENT**

513 This work was funded by the Korea Meteorological Administration Research and Development  
514 Program "Research and Development for KMA Weather, Climate, and Earth system Services–  
515 Development of Monitoring and Analysis Techniques for Atmospheric Composition in Korea"  
516 under Grant (1365003041).

517

518 **REFERENCES**

519 Akagi, S. K., R. J. Yokelson, C. Wiedinmyer, M. J. Alvarado, J. S. Reid, T. Karl, J. D. Crouse,  
520 P. O. Wennberg: Emission factors for open and domestic biomass burning for use in atmospheric  
521 models, *Atmos. Chem. Phys.* 11, 4039-4027, doi:10.5194/acp-11-4039-2011, **2011**



- 522 Chen, Y. Y. Li: Low-carbon economy and China's regional energy use research. *Jilin Univ. J.*  
523 *Soc. Sci. Ed.* 49(2), 66-73, **2009**
- 524 Fang, X., R. L. Thompson, T. Saito, Y. Yokouchi, J. Kim, S. Li, K. R. Kim, S. Park, F. Graziosi,  
525 A. Stohl: Sulfur hexafluoride (SF<sub>6</sub>) emissions in East Asia determined by inverse modeling.  
526 *Atmos. Chem. Phys.* 14, 4779–4791, doi:10.5194/acp-14-4779-2014, **2014**
- 527 Fu, X. W., H. Zhang, C.-J. Lin, X. B. Feng, L. X. Zhou, S. X. Fang: Correlation slopes of  
528 GEM/CO, GEM/CO<sub>2</sub>, and GEM/CH<sub>4</sub> and estimated mercury emissions in China, South Asia, the  
529 Indochinese Peninsula, and Central Asia derived from observations in northwestern and  
530 southwestern China. *Atmos. Chem. Phys.* 15, 1013-1028, doi:10.5194/acp-15-1013-2015, **2015**
- 531 Gamnitzer, U., U. Karstens, B. Kromer, R. E. M. Neubert, H. Schroeder, I. Levin: Carbon  
532 monoxide: A quantitative tracer for fossil fuel CO<sub>2</sub>?. *J. Geophys. Res.*, 111, D22302,  
533 doi:10.1029/2005JD006966, **2006**
- 534 Geller, L. S., J. W. Elkins, J. M. Lobert, A. D. Clarke, D. F. Hurst, J. H. Butler, R. C. Myers:  
535 Tropospheric SF<sub>6</sub>: Observed latitudinal distribution and trends, derived emissions and  
536 interhemispheric exchange time. *Geophys. Res. Lett.*, 24(6), 675–678, doi:10.1029/97GL00523,  
537 **1997**
- 538 Graven, H. D. N. Gruber: Continental-scale enrichment of atmospheric <sup>14</sup>CO<sub>2</sub> from the nuclear  
539 power industry: Potential impact on the estimation of fossil fuel-derived CO<sub>2</sub>. *Atmos. Chem.*  
540 *Phys. Discuss.* 11, 14,583–14,605, doi:10.5194/acpd-11-14583-2011, **2011**
- 541 Graven, H. D., B. B. Stephens, T. P. Guilderson, T. L. Campos, D. S. Schimel, J. E. Campbell, R.  
542 F. Keeling: Vertical profiles of biospheric and fossil fuel-derived CO<sub>2</sub> and fossil fuel CO<sub>2</sub>:CO



- 543 ratios from airborne measurements of  $^{14}\text{C}$ ,  $\text{CO}_2$  and  $\text{CO}$  above Colorado, USA, *Tellus*, *61*, 536–  
544 546, DOI:10.1111/j.1600-0889.2009.00421.x, **2009**
- 545 Gregg, J. S. R. J. Andres, G. Marland: China: Emissions pattern of the world leader in  $\text{CO}_2$   
546 emissions from fossil fuel consumption and cement production, *Geophys. Res. Lett.* *35*, L08806,  
547 doi:10.1029/2007GL032887, **2008**
- 548 Greenhouse Gas Inventory and Research Center: National Greenhouse Gas Inventory Report of  
549 Korea; National statistics-115018, 11-1480906-000002-10,  
550 [www.gir.go.kr/home/index.do?menuId=36](http://www.gir.go.kr/home/index.do?menuId=36) (in Korean), **2018**
- 551 Hsueh, D. Y., N. Y. Krakauer, J. T. Randerson, X. Xu, S. E. Trumbore, J. R. Southon: Regional  
552 patterns of radiocarbon and fossil fuel derived  $\text{CO}_2$  in surface air across North America, *Geophys.*  
553 *Res. Lett.*, *34*, L02816, doi:10.1029/2006GL027032, **2007**
- 554 Janssens-Maenhout, G., M. Crippa, D. Guizzardi, M. Muntean, E. Schaaf, J.G.J. Olivier,  
555 J.A.H.W. Peters, K.M. Schure: Fossil  $\text{CO}_2$  and GHG emissions of all world countries, EUR  
556 28766 EN, Publications Office of the European Union, Luxembourg, ISBN 978-92-79-73207-2,  
557 doi:10.2760/709792, JRC107877, **2017**
- 558 Janssens-Maenhout, G.; M. Crippa, D. Guizzardi, M. Muntean, E. Schaaf, F. Dentener, P.  
559 Bergamaschi, V. Pagliari, J. G. J. Olivier, J. A. H. W. Peters, J. A. van Aardenne, S. Monni, U.  
560 Doering, A. M. R. Petrescu, E. Solazzo, G. D. Oreggioni: EDGAR v4.3.2 Global Atlas of the  
561 three major greenhouse gas emissions for the period 1970–2012, *Earth Syst. Sci. Data*, *11*, 959–  
562 1002, <https://doi.org/10.5194/essd-11-959-2019>, **2019**



- 563 Kurokawa, J., T. Ohara, T. Morikawa, S. Hanayama, G. Janssens-Maenhout, T. Fukui, K.  
564 Kawashima, H. Akimoto: Emissions of air pollutants and greenhouse gases over Asian  
565 regions during 2000–2008: Regional Emission inventory in ASia (REAS) version 2, *Atmos.*  
566 *Chem. Phys.* *13*, 11019–11058, doi:10.5194/acp-13-11019-2013, **2013**
- 567 Labzovskii, L.D., H. W. L. Mak, S. T. Keneaa, J.-S. Rhee, A. Lashkari, S. Li, T.-Y. Goo, Y.-S.  
568 Oh, Y.-H. Byun: What can we learn about effectiveness of carbon reduction policies from  
569 interannual variability of fossil fuel CO<sub>2</sub> emissions in East Asia? *Environ. Sci. Policy.* *96*, 132-  
570 140, <https://doi.org/10.1016/j.envsci.2019.03.011>, **2019**
- 571 Lee, H., S.-O. Han, S.-B. Ryoo, J.-S. Lee, G.-W. Lee: The measurement of atmospheric CO<sub>2</sub> at  
572 KMA GAW regional stations, its characteristics, and comparisons with other East Asian sites.  
573 *Atmos. Chem. Phys.* *19*, 2149–2163, doi.org/10.5194/acp-19-2149-2019, **2019**
- 574 Lehman, S.J., J. B. Miller, C. Wolak, J.R. Southon, P.P. Tans, S.A. Montzka, C. Sweeney, A. E.  
575 Andrews, B.W. LaFranchi, T. P. Guilderson: Allocation of terrestrial carbon sources using <sup>14</sup>CO<sub>2</sub>:  
576 methods, measurement, and modelling. *Radiocarbon.* *55*(2–3):1484–95, **2013**
- 577 Le Quéré, C., R. M. Andrew, P. Friedlingstein, S. Sitch, J. Hauck, J. Pongratz, P. A. Pickers, J. I.  
578 Korsbakken, G. P. Peters, J. G. Canadell, A. Arneeth, V. K. Arora, L. Barbero, A. Bastos, L. Bopp,  
579 F. Chevallier, L. P. Chini, P. Ciais, S. C. Doney, T. Gkritzalis, D. S. Goll, I. Harris, V. Haverd, F.  
580 M. Hoffman, M. Hoppema, R. A. Houghton, G. Hurtt, T. Ilyina, A. K. Jain, T. Johannessen, C. D.  
581 Jones, E. Kato, R. F. Keeling, K. K. Goldewijk, P. Landschützer, N. Lefèvre, S. Lienert, Z. Liu,  
582 D. Lombardozzi, N. Metzl, D. R. Munro, J. E. M. S. Nabel, S. Nakaoka, C. Neill, A. Olsen, T.  
583 Ono, P. Patra, A. Peregón, W. Peters, P. Peylin, B. Pfeil, D. Pierrot, B. Poulter, G. Rehder, L.  
584 Robertson, E.M. Rocher, C. Rödenbeck, U. Schuster, J. Schwinger, R. Séférian, I. Skjelvan, T.



- 585 Steinhoff, A. Sutton, P. P. Tans, H. Tian, B. Tilbrook, F. N. Tubiello, I. T. vander Laan-Luijkx,  
586 G. R. vander Werf, N. Viovy, A. P. Walker, A.J. Wiltshire, R. Wright, S. Zaehle, Bo. Zheng:  
587 Global Carbon Budget 2018. *Earth Syst. Sci. Data*. 10, 2141–2194, <https://doi.org/10.5194/essd->  
588 [10-2141-2018](https://doi.org/10.5194/essd-10-2141-2018), **2018**
- 589 Levin, I., B., M. S. Kromer, H. Sartorius: A novel approach for independent budgeting of fossil  
590 fuel CO<sub>2</sub> over Europe by <sup>14</sup>CO<sub>2</sub> observations, *Geophys. Res. Lett.* 30(23), 2194,  
591 doi:10.1029/2003GL018477, **2003**
- 592 Li, S., J. Kim, S. Park, S.-K. Kim, M.-K. Park, J. Mühle, G.-W. Lee, M. Lee, C. O. Jo, K.-R.  
593 Kim: Source identification and apportionment of halogenated compounds observed at a remote  
594 site in East Asia. *Eviron. Sci. Technol.* 48, 491–498, doi.org/10.1021/es402776w, **2014**
- 595 Miller, J.B., S. J. Lehman, S. A. Montzka, C. Sweeney, B. R. Miller, A. Karion, C. Wolak, E. J.  
596 Dlugokencky, J. Southon, J. C. Turnbull, P.P. Tans: Linking emissions of fossil fuel CO<sub>2</sub> and  
597 other anthropogenic trace gases using atmospheric <sup>14</sup>CO<sub>2</sub>. *J. Geophys. Res.* 117, D08302,  
598 doi:10.1029/2011JD017048, **2012**
- 599 Niu, Z., W. Zhou, X. Feng, T. Feng, S. Wu, P. Cheng, X. Lu, H. Du, X. Xiong, Y. Fu:  
600 Atmospheric fossil fuel CO<sub>2</sub> traced by <sup>14</sup>CO<sub>2</sub> and air quality index pollutant observations in  
601 Beijing and Xiamen, China. *Environ. Sci. Pollut. Res.* 25, 17109–17117,  
602 doi.org/10.1007/s11356-018-1616-z, **2018**
- 603 Niu, Z., W. Zhou, P. Cheng, S. Wu, X. Lu, X. Xiong, H. Du, Y. Fu: Observations of atmospheric  
604 Δ<sup>14</sup>CO<sub>2</sub> at the global and regional background sites in China: Implication for fossil fuel CO<sub>2</sub>  
605 inputs. *Eviron. Sci. Technol.* 50, 12122–12128 DOI: 10.1021/acs.est.6b02814, **2016**



- 606 Nydal, R., and K. Lövseth, Carbon-14 measurements in atmospheric CO<sub>2</sub> from Northern and  
607 Southern Hemisphere sites, 1962–1993, technical report, *Carbon Dioxide Inf. Anal. Cent., Oak*  
608 *Ridge Natl. Lab.*, U.S. Dep. of Energy, Oak Ridge, Tenn, **1996**
- 609 Rafter, T. A., and G. J. Fergusson, “Atom Bomb Effect”—Recent increase of Carbon-14 content  
610 of the atmosphere and biosphere, *Science*, 126(3273), 557–558, **1957**
- 611 Palstra, S. W., U. Karstens, H.-J. Streurman, H. A. J. Meijer: Wine ethanol <sup>14</sup>C as a tracer for  
612 fossil fuel CO<sub>2</sub> emissions in Europe: Measurements and model comparison, *J. Geophys. Res.*,  
613 *113*, D21305, doi:10.1029/2008JD010282, **2008**
- 614 Riley, W. G., D. Y. Hsueh, J. T. Randerson, M. L. Fischer, J. Hatch, D. E. Pataki, W. Wang, M.  
615 L. Goulden: Where do fossil fuel carbon dioxide emissions from California go? An analysis  
616 based on radiocarbon observations and an atmospheric transport model, *J. Geophys. Res.*, *113*,  
617 G04002, doi:10.1029/2007JG000625, **2008**
- 618 Rivier, L., P. Ciais, D. A. Hauglustaine, P. Bakwin, P. Bousquet, P. Peylin, A. Klonecki:  
619 Evaluation of SF<sub>6</sub>, C<sub>2</sub>Cl<sub>4</sub>, and CO to approximate fossil fuel CO<sub>2</sub> in the Northern Hemisphere  
620 using a chemistry transport model. *J. Geophys. Res.* 111, D16311, doi:10.1029/2005JD006725,  
621 **2006**
- 622 Suntharalingam, P., D. J. Jacob, P. I. Palmer, J. A. Logan, R.M. Yantosca, Y. Xiao, M. J. Evans:  
623 Improved quantification of Chinese carbon fluxes using CO<sub>2</sub>/CO correlations in Asian outflow, *J.*  
624 *Geophys. Res.* 109, D18S18, doi:10.1029/2003JD004362, **2004**
- 625 Suess, H. E. Radiocarbon concentration in modern wood, *Science*, 122,415, **1955**



- 626 Stuiver, M., P. Quay: Atmospheric  $^{14}\text{C}$  changes resulting from fossil fuel  $\text{CO}_2$  release and cosmic  
627 ray flux variability, *Earth Planet. Sci. Lett.* 53, 349–362, **1981**
- 628 Tang, W., A. F. Arellano, J. P. DiGangi, Y. Choi, G. S. Diskin, A. Agustí-Panareda, M.  
629 Parrington, S. Massart, B. Gaubert, Y. Lee, D. Kim, J. Jung, J. Hong, J.-W. Hong, Y. Kanaya, M.  
630 Lee, R. M. Stauffer, A. M. Thompson, J. H. Flynn, J.-H. Woo: Evaluating high-resolution  
631 forecasts of atmospheric CO and  $\text{CO}_2$  from a global prediction system during KORUS-AQ field  
632 campaign. *Atmos. Chem. Phys.* 18, 11007–11030, doi.org/10.5194/acp-18-11007-2018, **2018**
- 633 Tans, P. P.; J. A. Berry, R. F. Keeling: Oceanic  $^{13}\text{C}/^{12}\text{C}$  observations: A new window on ocean  
634  $\text{CO}_2$  uptake. *Global Biogeochem. Cycles.* 7(2), 353–368, doi:10.1029/93GB00053, **1993**
- 635 Stuiver, M., Polach H. A. Discussion: Reporting of  $^{14}\text{C}$  data, *Radiocarbon*, 19(3), 355–363, **1977**
- 636 Tans, P.P., A.F.M. de Jong, W.G. Mook: Natural atmospheric  $^{14}\text{C}$  variation and the Suess effect,  
637 *Science*, 280, 826-828, **1979**
- 638 Thoning, K. W., P. P. Tans, W. D. Komhyr: Atmospheric Carbon dioxide at Mauna Loa  
639 Observatory 2. Analysis of the NOAA GMCC Data, 1984–1985, *J. Geophys. Res.* 94, 8549–  
640 8565, **1989**
- 641 Tohjima, Y., M. Kubo, C. Minejima, H. Mukai, H. Tanimoto, A. Ganshin, S. Maksyutov, K.  
642 Katsumata, T. Machida, K. Kita: Temporal changes in the emissions of  $\text{CH}_4$  and  $\text{CO}$  from China  
643 estimated from  $\text{CH}_4/\text{CO}_2$  and  $\text{CO}/\text{CO}_2$  correlations observed at Hateruma Island. *Atmos. Chem.*  
644 *Phys.* 14, 1663–1677, doi:10.5194/acp-14-1663-2014, **2014**



- 645 Turnbull, J., P. Rayner, J. Miller, T. Naegler, P. Ciais, A. Cozic: On the use of  $^{14}\text{CO}_2$  as a tracer  
646 for fossil fuel  $\text{CO}_2$ : Quantifying uncertainties using an atmospheric transport model, *J. Geophys.*  
647 *Res. 114*, D22302, doi:10.1029/2009JD012308, **2009**
- 648 Turnbull, J. C., S. J. Lehman, J. B. Miller, R. J. Sparks, J. R. Southon, P. P. Tans: A new high  
649 precision  $^{14}\text{CO}_2$  time series for North American continental air. *J. Geophys. Res. 112*, D11310,  
650 doi:10.1029/2006JD008184, **2007**
- 651 Turnbull, J. C., P. P. Tans, S. J. Lehman, D. Baker, T. J. Conway, Y. S. Chung, J. Gregg, J. B.  
652 Miller, J. R. Southon, L.-X. Zhou: Atmospheric observations of carbon monoxide and fossil fuel  
653  $\text{CO}_2$  emissions from East Asia. *J. Geophys. Res.*, *116*, D24306, doi:10.1029/2011JD016691,  
654 **2011a**
- 655 Turnbull, J. C., A. Karion, M. L. Fischer, I. Faloona, T. Guilderson, S. J. Lehman, B. R. Miller, J.  
656 B. Miller, S. Montzka, T. Sherwood, S. Saripalli, C. Sweeney, P. P. Tans: Assessment of fossil  
657 fuel carbon dioxide and other anthropogenic trace gas emissions from airborne measurements  
658 over Sacramento, California in spring 2009, *Atmos. Chem. Phys. 11(2)*, 705–721,  
659 doi:10.5194/acp-11-705-2011, **2011b**
- 660 Turnbull, J. C. J. B. Miller, S. J. Lehman, P. P. Tans, R. J. Sparks, J. Southon: Comparison of  
661  $^{14}\text{CO}_2$ ,  $\text{CO}$ , and  $\text{SF}_6$  as tracers for recently added fossil fuel  $\text{CO}_2$  in the atmosphere and  
662 implications for biological  $\text{CO}_2$  exchange, *Geophys. Res. Lett.*, *33*, L01817,  
663 doi:10.1029/2005GL024213, **2006**



- 664 Wang, Y. J. W. Munger, S. Xu, M. B. McElroy, J. Hao, C. Nielsen, H. Ma: CO<sub>2</sub> and its  
665 correlation with CO at a rural site near Beijing: Implications for combustion efficiency in China,  
666 *Atmos. Chem. Phys.* 10, 8881–8897, doi:10.5194/acp-10-8881-2010, **2010**
- 667 Yin, L., P. Du, M. Zhang, M. Liu, T. Xu, Y. Song: Estimation of emissions from biomass  
668 burning in China (2003–2017) based on MODIS fire radiative energy data, *Biogeosciences*, 16,  
669 1629–1640. **2019**